Journal of Himalayan Earth Sciences Volume 49, No. 2, 2016, pp. 137-157

Petrography and Whole-Rock Geochemistry of the Oligocene-Miocene Khojak Formation Khojak-Pishin Belt, Pakistan: Implications on Provenance and Source Area Weathering

Din Muhammad Kakar[1], Aimal Khan Kasi[2*], Akhtar Muhammad Kassi[1], Henrik Friis[3], Mohibullah Mohibullah[1] and Suleman Khan[4]

[1]Department of Geology, University of Balochistan, Quetta, Pakistan
[2]Centre of Excellence in Mineralogy, University of Balochistan, Quetta, Pakistan
[3]Department of Geoscience, Aarhus University, Denmark
[4]Department of Geology, University of Peshawar
[*]Corresponding author's email: aimal_kai@yahoo.co.uk

Abstract

The Oligocene and Early Miocene Khojak Formation represent a deltaic to sub-marine fan succession in the Khojak-Pishin flysch belt within the Katawaz basin of Pakistan. The sandstone within this succession is dominated by sedimentary and metamorphic clasts and has been derived from recycled orogeny. The higher SiO_2/Al_2O_3 ratios (4.0) show moderately mature nature of the sandstone. The weathering indices such as Chemical Index of Alteration (CIA; 76.69), Chemical Index of Weathering (CIW; 86.79), Chemical Proxy of Alteration (CPA; 92.33) and Index of Chemical Variability (ICV; 16.83) suggest moderate to intense weathering at the source terrain. The high Th/U values (5.25) as compared to Upper Continental Crust (UCC; 3.82) also support the enhanced weathering of the source area. Trace elements such as Zr, Nb, Y, Th and U are slightly enriched compared to UCC suggest the dominantly felsic sources for the formation. High enrichment of Cr, Ni and V, and moderate ratios of Cr/Ni (1.72) and Cr/V (1.83) indicate substantial contributions from ultramafic sources while fairly high percentages of Fe_2O_3 (7.66) and MgO (3.90) as compared to UCC (5.03% and 2.20%, respectively) hints toward mafic sources. The tectonic setting for the Khojak sandstone is considered as continental arc to active continental margin. This study supports the notion that the western Himalayan orogenic belt was shedding largely felsic detritus to Katawaz basin through proto-Indus River, while mafic and ultramafic detritus were being fed by distant Kohistan Island Arc and en-route Waziristan, Zhob and Muslim Bagh Ophiolite and associated mélanges. The sediment dispersal towards south-southwest was controlled by Chaman-Nushki transform fault system.

Keywords: Khojak Formation; Katawaz basin; Recycled orogeny

1. Introduction

The early collision of Indian and Eurasian plates, between 66 and 55 Ma has resulted in the crustal thickening and uplift of orogenic highlands, hence the initiation of Himalayas (Beck et al., 1995; Klootwijk et al., 1992). Pre-collision subduction has closed the northern part of the Neo-Tethys Ocean between the two plates, and opened Katawaz Ocean (now comprising Katawaz belt in Afghanistan and Khojak-Pishin Belt in Pakistan) in the southwest, which was a remnant ocean of former Neo-Tethys (Qayyum et al., 1997a). The northwestern part of nascent Himalayas started shedding detritus which was subsequently taken away by the major drainage system and deposited on to the forelands of Himalayas as fluvial deposits and further taken to deltas at continental margins that were axially feeding submarine fan in deep ocean (Graham et al., 1975; Qayyum et al., 1996; Kassi et al., 2011, 2015). Qayyum et al. (1996) considered Paleo-Indus River as a trunk river that eroded and transported the Palaeogene siliciclastic detritus from western flanges of Himalayas to Katawaz delta-submarine fan succession (e.g. Critelli et al., 1990; Kassi et al., 2011; 2015). The Oligocene-Early Miocene deltaic and submarine fan successions (Khojak and Panjgur formations respectively) in the Pishin, Khojak and Makran belts of Pakistan represent a gigantic delta-submarine fan system which resembled the modern Indus delta-fan system. The Panjgur Formation is exposed in central and northern Makran of Pakistan and Iran, and it represents the submarine fan of delta-submarine fan system (McCall and Kidd, 1982;

Kassi et al., 2011; 2015). The tectonic uplift of the Kirthar Fold-Thrust belt during Miocene has resulted in the shift of the fan to the east (Clift et al., 2001) i.e. to its current location (Fig. 1).

The petrography and geochemistry of sandstones are the reliable tools to determine provenance, climate and tectonic/ palaeogeographic settings of the source area and depositional basin (Basu, 1985; McLennan, 2001). The detrital modes of sandstone of the Khojak Formation within the Pishin Belt were documented by Qayyum et al. (2001). The present paper is first of its kind which focuses mainly on the elemental geochemistry of sandstones of the Khojak Formation. This study will enhance our understanding of the provenance and tectonic setting of the formation in question.

2. Geology of the area

The Khojak Formation is well exposed in the northeast-southwest trending Khojak-Pishin flysch Belt (Fig. 2). The 6300 m thick monotonous sequence of the Khojak Formation is comprised of two members; the lower Murgha Faqirzi Member, comprising of regularly bedded sandstone and shale (Jones, 1960; Qayyum et al., 1996). In the Makran area, the equivalent unit is composed of distal turbidites (Platt and leggett, 1986; Critelli et al., 1990; Kassi et al., 2011, 2015). The upper Shaigalu Member is dominantly composed of fluvial-wave dominated deltaic sandstone (Qayyum et al., 1996; Carter et al., 2010). Based on the recovered fossils from its middle and upper parts, Late Eocene to Early Miocene age has been assigned (Jones, 1961; Iqbal and Shah, 1980; Qayyum et al., 1996).

The Pishin Belt stretches 700 km along its length and 200 km along its width and has archives ~8 km thick carbonate and siliciclastic succession (Fig. 2). The north-south trending Khojak block bends near the Quetta into north-east-trending and south-east-convex Pishin Belt (Powell, 1979; Sarwar and DeJong, 1979; Bender and Raza, 1995). The Chaman-Nushki Fault bound the Khojak-Pishin belt in west marking a transform boundary with the Afghan Block, whereas the Zhob Valley Thrust bound the belt to the east. Most of the transform motion between Eurasia and India is accommodated along ~ 900 km long Ornach-Nushki-Chaman Fault (Lawrence et al., 1981; Jadoon and Khurshid, 1996). The Zhob Valley Thrust translates the entire belt east and southeast over the Muslim Bagh-Zhob Ophiolite and western passive margin of the Indian Plate (Lawrence and Yeats, 1979; Lawrence et al., 1981; Treloar and Izatt, 1993; Bender and Raza, 1995; Jadoon and Khurshid, 1996; Kazmi and Jan, 1997). The belt is characterized by tight anticlines and wide synclines, suggesting transpressional to compressional deformation from western edge to the eastern limits (Iqbal, 2004).

The belt evolved as a result of the early collision of north-drifting Indian Plate with Eurasian Plate during Late Paleocene-Early Eocene time. The cessation of Neo-Tethys as a result of the northern collision has subsequently resulted in the opening of the Katawaz Ocean in southwest which is considered as remnant part of the Neo-Tethys. The Katawaz remnant ocean was ultimately closed by the end of Early Miocene and the Indian and Eurasian plates finally sutured in the west (Qayyum et al., 1997a; 2001). A very thick sedimentary (mainly terrigeneous and subordinately marine) succession fills the Katawaz Basin. The Khojak-Pishin Belt include Cretaceous-Paleocene Muslim Bagh-Zhob Ophiolite, Eocene Nisai Formation, Oligocen Khojak Formation, Miocene-Early Dasht Murgha Group, Pliocene Malthanai Formation and Pleistocene Bostan Formation (Kasi et al., 2012) (Table 1).

3. Methodology

3.1. Samples

Fresh and pristine sandstone samples were obtained from various outcrop sections of the study area, such as Kishingi, Sher Jan Agha, Kirdigab (near Nushki), Panjpai, Spina Tizha, Lajwar, Arambai, Khojak Pass (Chaman), Tor Tangi (near Barshore) Ragha Bukalzai (near Muslim Bagh), Murgha Faqirzai (near Nisai) and Shegalu (west of Zhob) (Fig. 2).

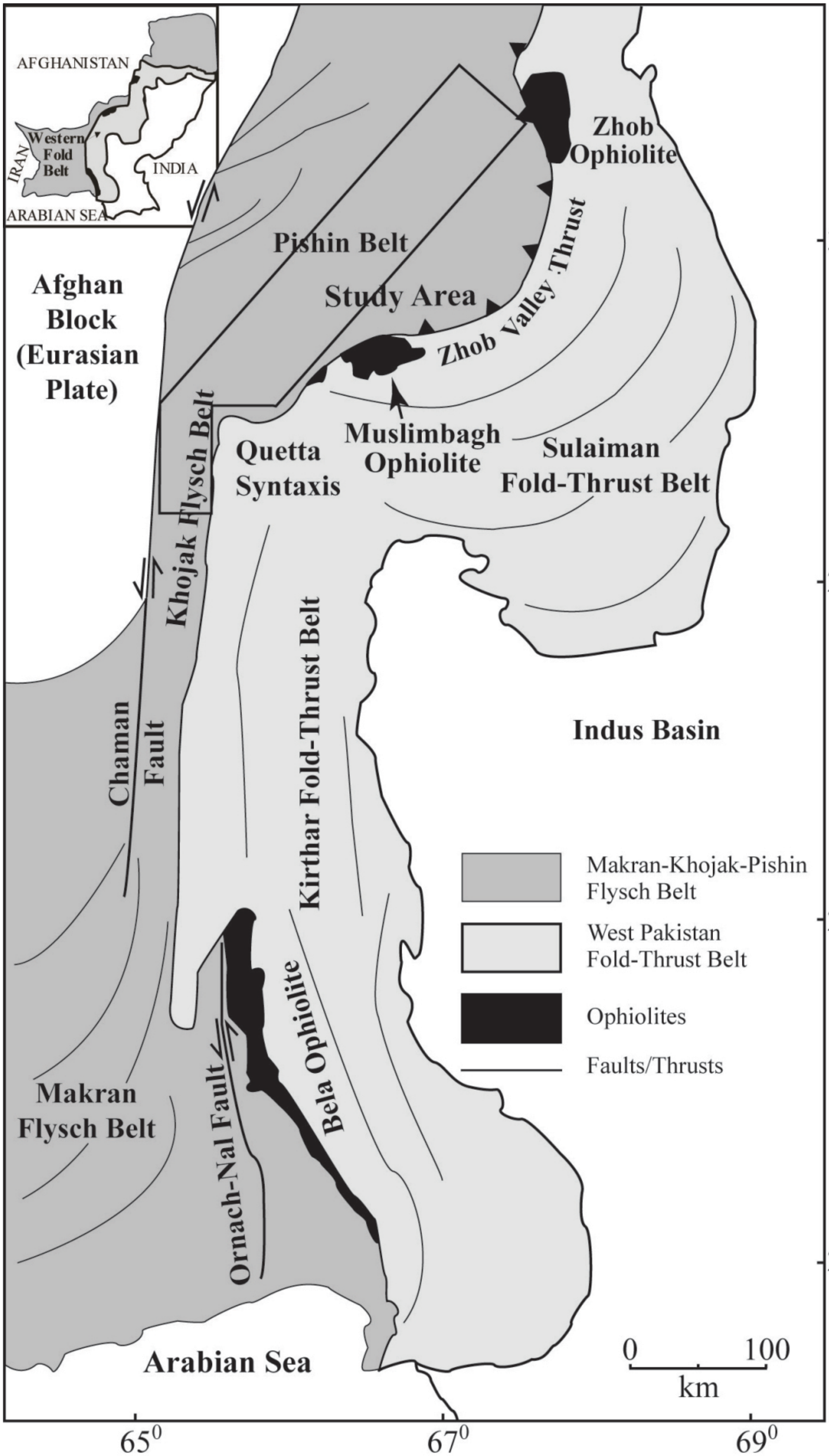

Fig. 1. Generalized geological map of the western side of Pakistan showing the position of Pishin and Khojak belts and study area.

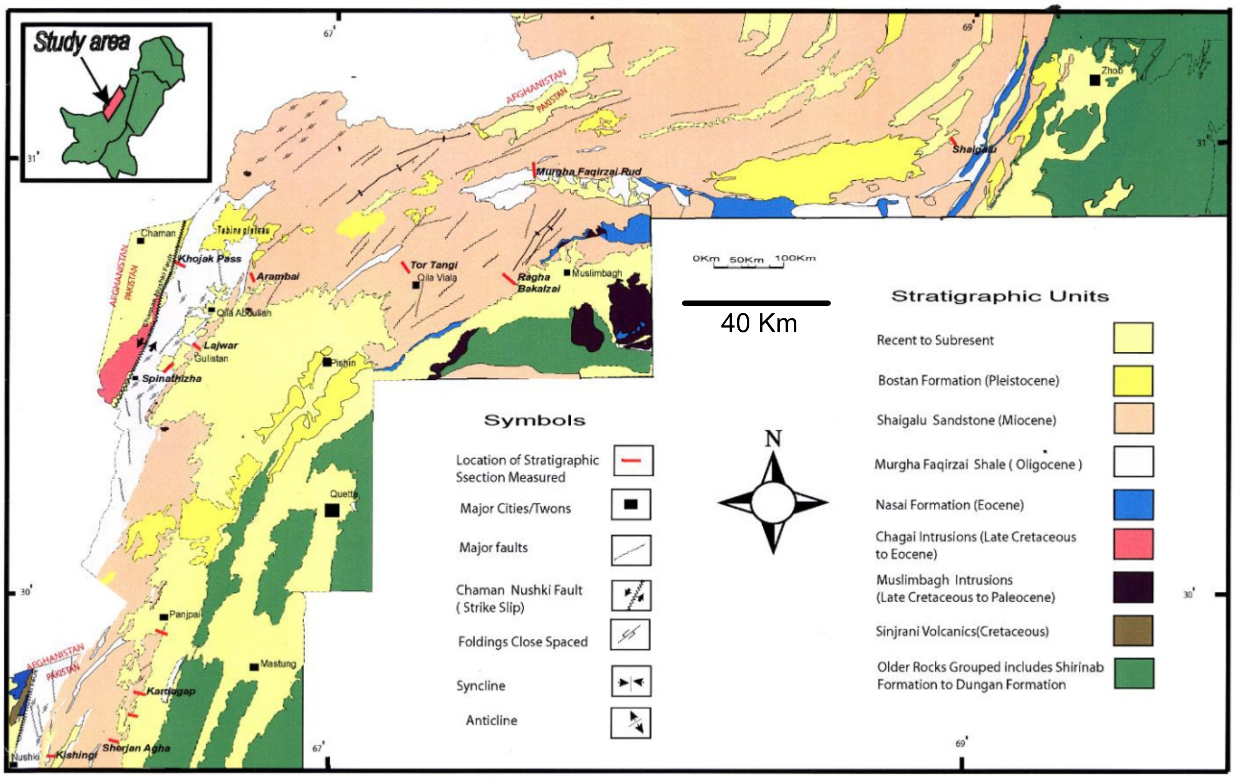

Fig. 2. Geological map of the study area, showing measured sections.

The earthquake records can be divided into two reigns, first before the invention of sophisticated instruments often called as historical earthquakes, second the earthquakes recorded after the invention of sophisticated instruments are known as Instrumental earthquake record. Historical earthquake record for study area is shown in Table 1. Instrumental earthquake record for the region is obtained from International Seismological Center (ISC), shown in Figure 4.

3.2. Analytical methods

A total of 36 standard thin sections were prepared and studied using Olympus BX 51 polarizing microscope at the Centre of Excellence in Mineralogy, University of Balochistan, Pakistan. The geochemical investigations were carried out on 41 sandstone samples from 6 different widely located stratigraphic sections. X-ray fluorescence spectrometer (Philips PW 2400 XRF) was used to determine major and trace elements using fused disks and pressed pellets respectively at the Department of Geosciences, Aarhus University, Denmark. Oxides of major elements (SiO_2, TiO_2, Al_2O_3, Fe_2O_3[Total], MnO, MgO, CaO, Na_2O, K_2O and P_2O_5) and trace elements (Ni, Cu, Zn, Rb, Sr, Y, Zr, Nb, Pb, Th, U, Ba, La, Ce, V and Cr) were utilized in this study. A strong correlation exists between LOI and CaO, indicating that the amount of LOI caused by calcite can be determined. The amount of CaO, which is not carried by calcite is very small, 1% or less. It is assumed that most of CaO is bound by calcite and, therefore, the CaO value is arbitrarily set in the "sandstone part" to 1% and then calculated the remnant CaO as calcite and associated part of volatiles and subtracted this part from the total LOI. Afterward the composition was normalized on volatile-free basis. Trace elements have also been normalized by dividing the normalized SiO_2 by original SiO_2 for each sample.

3. Petrology

The sandstone of Khojak Formation ranges from very coarse to very fine-grained. The grains are sub-angular to sub-rounded and moderately to poorly sorted (Fig. 3a). Most of the samples have grain-supported fabric. Some of the samples have cement-supported fabric while few samples with matrix-supported fabric were also observed. The grains with concavo-convex, sutured and straight contacts were observed.

4.1 Detrital constituents

Quartz is the most abundant mineral constituent of the studied sandstone, and it includes both monocrystalline and polycrystalline varieties of igneous and metamorphic affinity. The monocrystalline grains display both straight and undulose extinctions while the polycrystalline quartz has straight and sutured contacts. The polycrystalline quartz frequently shows preferred orientation of the constituent grains. The quartz overgrowths are observed in some of the quartz grains. The quartz grains often contain inclusions of vermicular chlorite (Fig. 3b), zircon, pyrite or iron oxides. The K-feldspar and plagioclase constitutes the second most abundant group (Fig. 3c). The K-feldspar dominates over plagioclase and includes orthoclase and microcline. The feldspar grains are recognizable on the basis of second-order grey interference colors, cloudy appearance, cleavage pattern and twinning while plagioclase displays albite-type twinning (Fig. 3b) and is present as single grains and as framework crystals within the crystalline lithic fragments. The perthite is also very common. The feldspar readily alters and this alteration ranges from partial to complete replacement by calcite, chlorite and clay minerals.

The sandstone has recorded varieties of igneous, metamorphic and sedimentary rock fragments (Table 2 and Fig. 3d). The lithics comprise the second most abundant group. Amongst the lithics the basic igneous rocks (basalt) are the most abundant while other igneous fragments include granite and gabbro. The muscovite and chlorite schist represent the dominant lithic fragment amongst the metamorphic rock fragments. Other metamorphic fragments include quartzite and gneiss. The sedimentary lithics include shale, mudstone, siltstone, sandstone, chert, limestone, chalcedony and fossil fragments are the dominant (Table 2). The incompetent lithic fragments e.g. shale, siltstone, phyllite, limestone and fossil fragments are sometimes squeezed and penetrated between other competent grains as a result of burial diagenesis.

Minor muscovite and biotite are commonly recorded in all the thin sections. The biotite is strongly pleo-chroitic (Fig. 3e). The biotite shows slight to complete alteration to chlorite. The chlorite is also a common mineral constituent of sandstone.

Heavy minerals include picotite, zircon, epidote, rutile, garnet, pyroxenes, amphiboles and tourmaline (Fig. 3f). The pyrite is most common among mineral amongst opaque minerals.

4.2 Modal composition and Provenance

Qayyum et al. (2001) carried out modal analysis of the Khojak Formation using 43 samples in Manzaki, Rud Faqirzai and Gardab Manda sections in the Khojak-Pishin Belt. In their study 13 recalculated parameters were used to plot five ternary diagrams of Dickinson and Suczek (1979), Ingersoll and Suczek (1979), Zuffa (1980), Dickinson et al. (1983) and Ingersoll et al. (1984). Sandstone is quartzolithic in composition and mean values of the QtFL and QmFLt are Qt60F09L31 and Qm47F10Lt43 respectively. In QtFL and QmFLt ternary diagrams the samples fall in the fields of recycled and transitional recycled orogens, respectively (Fig. 4a and b). Mean value of QmPK (Qm82P13K5) suggests the dominance of monocrystalline quartz over feldspars. Mean values of LmLvLs (Lm20Lv5Ls75) and QpLvmLsm (Qp24Lvm6Lsm70) suggest dominance of the sedimentary and meta-sedimentary detritus in sandstones (Qayyum et al. 2001, Figs. 5-7). Samples plot in the suture belt, and mixed magmatic arc and subduction complexes.

5. Geochemistry

5.1 Major elements

The concentrations of major and trace elements are presented in Table 3 and Table 4, respectively. For reference mean values of the Upper Continental Crust (UCC) are included in tables and figures (McLennan, 2001). Various elemental ratios are also given in Table 3 and Table 4. Sandstones exhibit significant variations in oxides of major elements (Table 3). SiO_2 has the highest weight percentages and show large variations (range: 59.11 - 84.31; average: 65.10). The sandstones are slightly depleted in SiO_2 when compared to UCC data (UCC: 66%; Table 3) (McLennan, 2001).

Table 1. Lithostratigraphy of the Pishin and Khojak belt (after Kasi et al., 2012).

Age	Group	Formation/Member		Lithology	Tectono-stratigraphic Zones
Holocene	-	Zhob River Deposits		Conglomerate, sandstone and shale/siltstone	Zone VI
Thrust/Angular Unconformity					
Pleistocene	-	Bostan Formation		Red colored shale/siltstone, conglomerate and sandstone	Zone V
Thurst/Angular Unconformity					
Late Miocene-Pliocene	-	Malthanai formation		Sandstone and conglomerate interbedded with red colored mudstone/siltstone	Zone IV
Thurst/Angular Unconformity					
Middle to Late Miocene	Dasht Murgha group	Sra Khula formation		Dark red mudstone dominated by cyclic alteration of mudstone, siltstone and sandstone	Zone III
		Bahlol Nika formation		Dominantly greyish green sandstone, with subordinate mudstone and occasional conglomerate	
		Khuzhobai formation		Dominantly maroon mudstone with subordinate reddish brown sandstone	
Thrust/Angular Unconformity					
Oligocene – Early Miocene	-	Khojak Formation	Shaigalu Member	Dominantly sandstone with subordinate shale	Zone II
			Murgha Faqirzai Member	Dominantly shale with subordinate sandstone	
Eocene	-	Nisai Formation		Highly fossiliferous to reefoid limestone interbedded with marl and thick marine (fossiliferous) shale with occasional thin limestone horizons	
Nonconformity					
Cretaceous	-	Muslim Bagh-Zhob Ophiolite		Mostly ultrabasic and basic igneous rocks	Zone I

Table 2. List of varieties of rock fragments present in sandstone of the Khojak Formation.

Igneous	Metamorphic	Sedimentary
Granite Muscovite–biotite granite	Quartzite	A variety of limestone fragments
	Gneissose quartzite	A variety of calcareous fossil fragments
Rhyolite	Muscovite schist	
Basalt	Muscovite–biotite schist	Calcarenite
Volcanic glass	Chlorite schist	Sandstone
Volcanic tuff	Gneiss	Siltstone
	Phyllite	Shale
Serpentine	Slate	Chert (radiolarian)
	Marble	

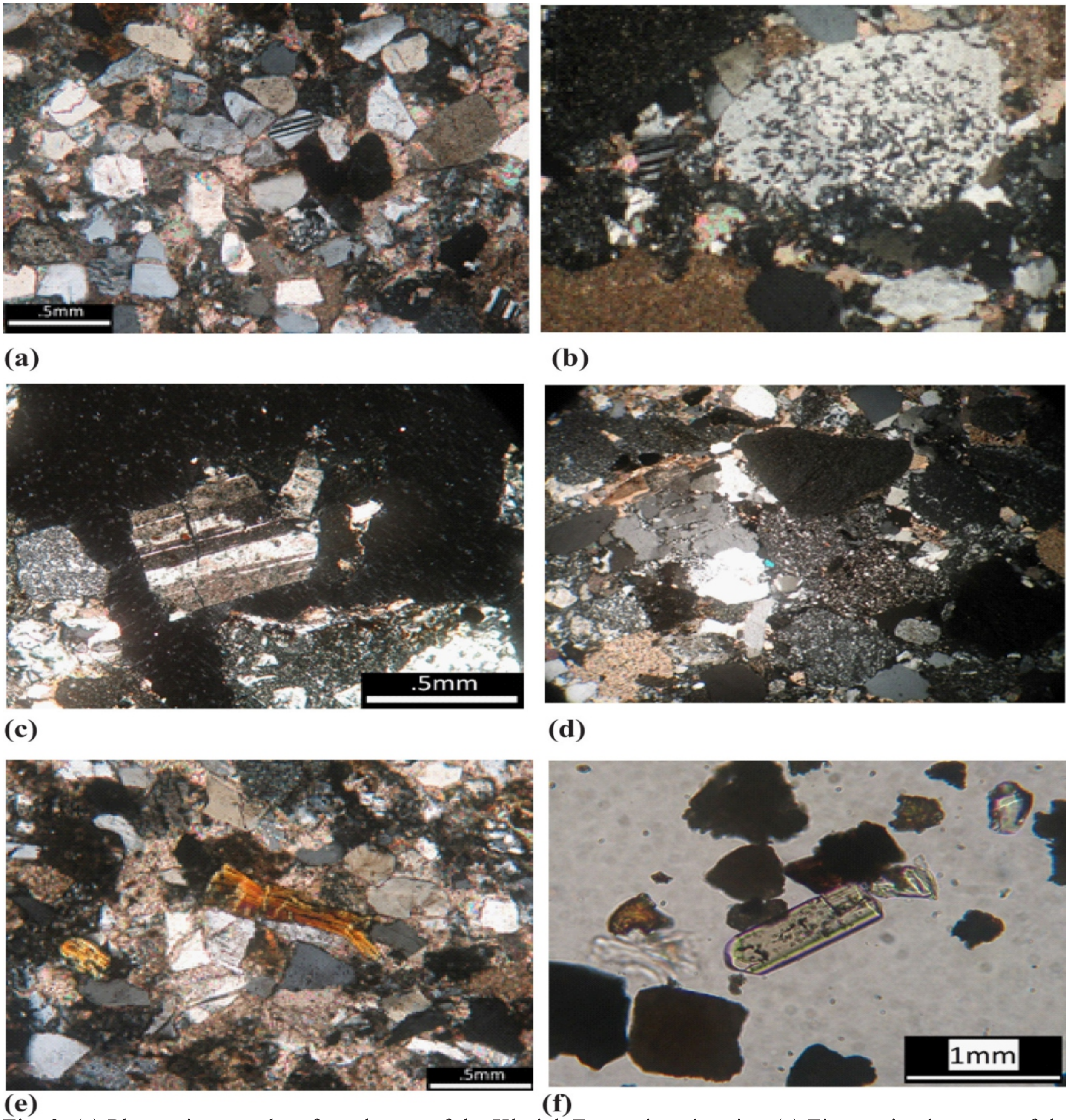

Fig. 3. (a) Photomicrographs of sandstone of the Khojak Formation showing (a) Fine grained texture of the sandstone, XP (b) Vermiculite inclusion in monocrystalline quartz grain, 10x20, XP; (c) Plagioclase having albite-type twinning in sandstone of the Khojak Formation, XP; (d) Chert and limestone fragments XP; (e) Biotite flakes; (f) Tourmaline grain in sandstone of the Khojak Formation, XP

Al_2O_3 has the second highest percentages (range: 6.87 - 20.95; mean: 17.07). The sandstone has higher SiO_2/A_l2O_3 ratios (range: 2.84 to 12.28; mean: 4.0); mean of the ratio is slightly less compared to UCC (4.34). This reflects the moderately mature nature of the sandstones, due to quartz enrichment, as also seen in the petrographic study. The formation has higher K_2O/Na_2O ratios (range: 0.60 - 7.04; mean: 2.21); mean ratio is much higher compared to UCC (0.87). Higher K_2O/Na_2O ratios reflect dominance of the Alkali feldspars over plagioclase. The mean percentages of Fe_2O_3 (7.66) and MgO (3.90) are fairly high as compared to UCC (5.03% and 2.20%, respectively). The higher percentages of the Fe_2O_3 and MgO (Fe_2O_3+MgO: 11.55; UCC: 7.23) along with the consistent ratios of TiO_2/Al_2O_3 (mean: 0.05), is attributed to the higher proportion of ferromagnesian minerals, derived from mafic and ultramafic rocks. The sandstones show slight enrichment in MnO (0.10; UCC 0.08), as a result of dilution effect of calcite cements and limestone fragments.

The bivariate plots are easy diagrams to correlate two variables (Harker, 1909; Bhatia, 1983; Ranjan and Banerjee, 2009). It may be noted that Al_2O_3 has strong positive correlation with TiO_2, Fe_2O_3, K_2O and P_2O_5 while CaO, MnO and Na_2O have negative correlation with Al_2O_3 (Fig. 5).

5.2 Sandstone classification

For the purpose of classification, schemes of Herron (1988) and Pettijohn et al. (1987) have been used (Figs. 6 and 7). In the Herron's (1988) classification scheme the analyzed samples make tight cluster and most of them plot inside the shale field in close proximity to the wacke field, whereas a couple of the samples plot in Fe-shale and Fe-sand again showing a close affinity to the shale and wacke (Fig. 6). This distribution is probably controlled by dilution of K_2O and moderately higher concentrations of Al_2O_3.

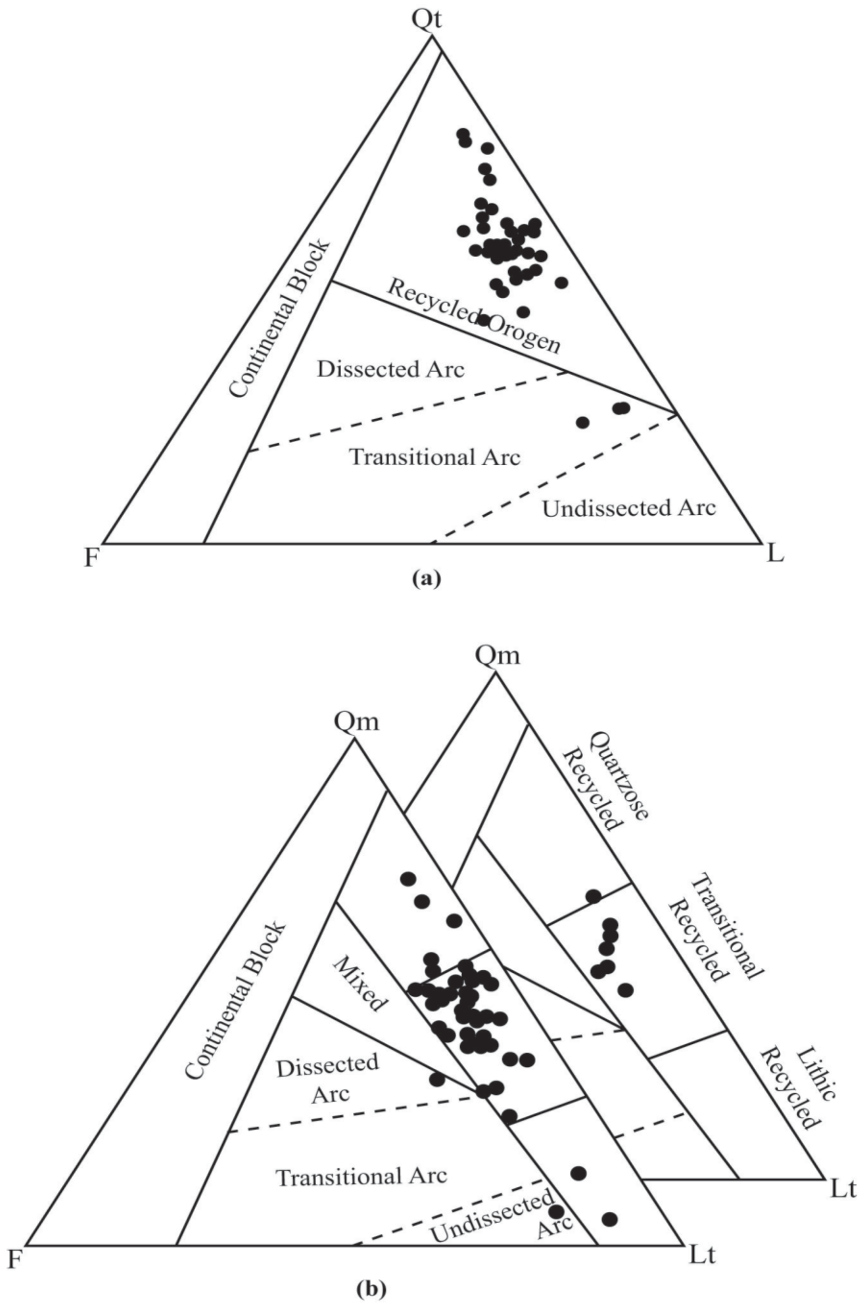

Fig. 4. (a) QtFL compositional diagram (after Dickinson and Suczek, 1979) for sandstones of the Khojak Formation (after Qayyum, 2001), (b) QmFLt compositional diagram (after Dickinson et al., 1983) of sandstones of the Khojak Formation (after Qayyum, 2001); ternary diagram in the background shows plots of the mean values

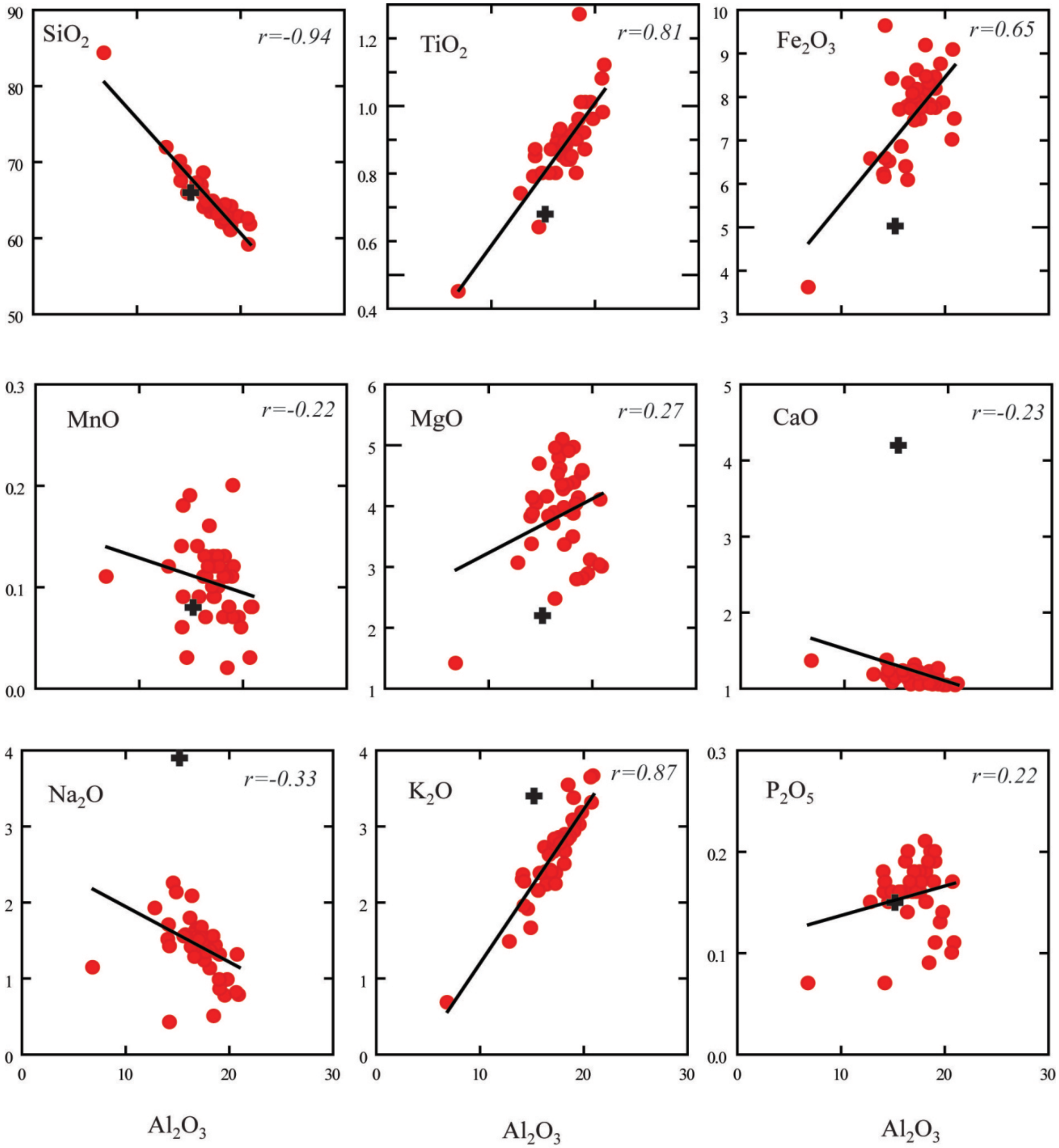

Fig. 5. Harker variation diagrams of various major elements vs Al2O3 (Bhatia, 1983) for sandstone samples of the Khojak Formation. Filled circles represent sandstones of the Khojak Formation and addition sign represents UCC values. r denotes correlation coefficents of the plotted data.

Pettijohn et al. (1987) classification scheme for sandstones, alternatively, put emphasize on K_2O/Na_2O ratios. In his scheme majority of the sandstone samples plot on the boundary between greywacke and litharenite field showing a tight linear pattern (Fig. 7). Some of the samples plot between the litharenite and arkose field and a couple plot inside the arkose. This classification also shows that higher K_2O and Al_2O_3 contents control distribution of the sandstone samples in the classification scheme.

5.3 Trace elements

Trace elements concentrations are given in Table 3. Ba has the highest mean value among the trace elements (mean: 305). Trace elements with higher concentrations in descending order include Cr (287), Zr (197), V (170), Sr (158) and Ni (166). The higher concentration of Zr and Cr is due to the presence of zircon and picotite. The sandstones of the Khojak Formation are highly depleted in Ba (UCC: 550) and Sr (UCC: 350). The depletion, compared to the UCC in Ba and Sr, is due to the weathering. The Zr and Rb are slightly enriched while Cr, Ni and V are highly enriched (UCC: Cr 83, Ni 44, V 107), which attest to substantial input from mafic and ultramafic detritus. The Cu, Zn, Ce, Th, Ga, Pb, La, Y, U and Nb have values higher than UCC.

The trace elements of the sandstone samples were also compared with Al_2O_3 for correlation purpose. It may be noted that Zn, Ba, Ni, Ce, La, Cu, Th, Rb, Y, Nb, Ga and V correlate very well with Al_2O_3, showing a linear trends (Fig. 8), however, Zr, U and Sr, weakly correlate with Al_2O_3.

5.4 Source area weathering

The CIA (Nesbitt and Young, 1982;1984), CIW (Harnois, 1988), CPA (Buggle et al., 2011) and ICV (Cox et al., 1995) have been used to determine weathering in the source area. The feldspars readily alter to clay minerals. Ca, Na and K are generally dissolved from feldspars to increase the alumina content in the weathered detritus (see e.g. Nesbitt and Young, 1982). The weathering intensity can be understood by calculating Chemical Index of Alteration CIA, using molecular proportions, as:

$$CIA= [Al_2O_3/ (Al_2O_3+CaO^*+Na_2O+K_2O)] \times 100.$$

Harnois (1988) argued against the CIA i.e. the K_2O is erratic during chemical weathering and leaches out during soil formation. He excluded the K_2O from the proposed Chemical Index of Weathering (CIW):

$$CIW = [Al_2O_3/(Al_2O_3+CaO^*+Na_2O)] \times 100.$$

"In the above indices, CaO* is meant to represent only CaO of silicate minerals". CIW of Harnois was modified by Cullers (2000), Cullers removed the CaO, which, he argued, poses a problem of "dilution effect" from calcite cement and/or limestone fragments. He proposed a new Chemical Index of Weathering (CIW'), involving only the molecular proportions of aluminium and sodium. The CIW' was renamed by Buggle et al. (2011) as Chemical Proxy of Alteration (CPA): CIW' or $CPA = [Al_2O_3/(Al_2O_3+Na_2O)] \times 100$.

Cox et al. (1995) proposed the Index of Chemical Variability (ICV) that measures the abundance of alumina relative to other major cations, which may be used for assessing the maturity of the mud rocks. The higher ICV values are characterized by compositionally immature first-cycle mud rocks deposited in tectonically active settings (see e.g. Van de Kemp and Leake, 1985):

$$ICV = [(Fe_2O_3+K_2O+Na_2O+CaO^*+MgO+MnO+TiO_2)/Al_2O_3])$$

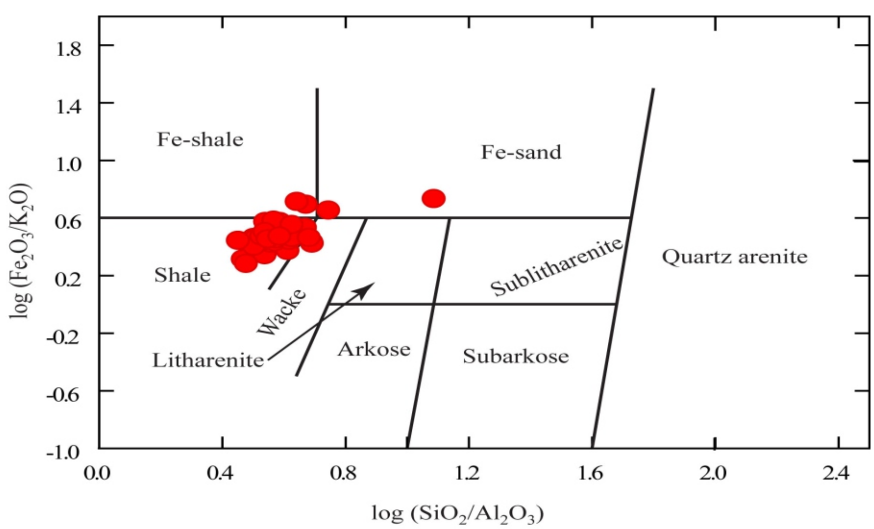

Fig. 6. Plot of the sandstone samples of the Khojak Formation, using classification diagram of log (Fe_2O_3/K_2O) vs log (SiO_2/ Al_2O_3) (after Herron, 1988).

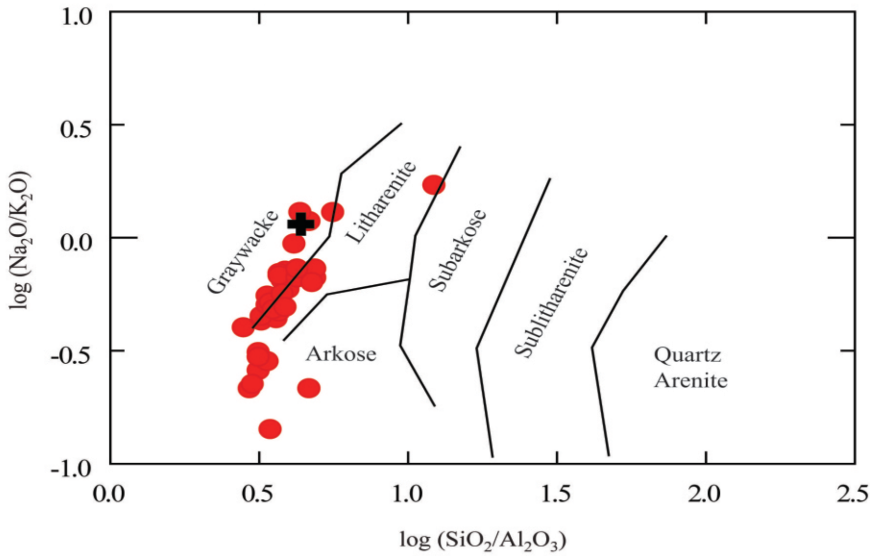

Fig. 7. Plot of the sandstone samples of the Khojak Formation, using classification diagram of log (Na_2O/K_2O) vs log (SiO_2/Al_2O_3) (after Pettijohn, 1987).

The above mentioned indices were calculated for sandstone samples of the Khojak Formation. The CIA values have a range from 68.38 to 80.25 with a mean of 76.69, indicating moderate to intense degree of weathering. The CIW ranges from 73.33 to 92.29 (mean 86.79) indicating moderate to highly intense weathered source terrain. The CPA shows a narrow range of 85.76 to 97.36 with a mean of 92.339, indicating a very strong weathering at the source terrain.

The ICV values of the sandstones range from 08.37 to 18.99, with a mean of 16.83. The ICV correspond to a field between K-feldspar (ICV: ~1) and chlorite (ICV: ~4) (see e.g. Cox et al., 1995). The sandstone contains a lower proportion of Al_2O_3 than clay minerals, therefore, having higher ICV values compared to clay minerals. The mature mudstone comprising mostly of clay minerals should display ICV values lower than 1.0 (Cox et al., 1995).

McLennan et al. (1993) proposed A-CN-K ($Al_2O_3CaO+Na_2O-K_2O$) and A-CNK-FM ($Al_2O_3CaO+Na_2O+K_2O-Fe_2O_3+MgO$) triangle diagrams to demonstrate increasing degree of weathering of felsic and mafic igneous rocks. These plots are used to gather bulk source composition and to assess the state of weathering (Nesbitt and Young, 1982;1984; Fedo et al., 1995; Nesbitt et al., 1996). The CIA values are commonly plotted over A-CN-K diagrams. The plots in this study show that most of the sandstone samples plot above the feldspar line in tight cluster between smectite and illite fields (Fig. 9a). This suggests a tectonically active source for the sediments; the detritus was derived from different zones of weathering profiles (e.g. Nesbitt et al., 1996). The A-CNK-FM diagram shows that the samples make even tighter cluster across the feldspar line, however, the samples plot very close to smectite on A-FM leg (Fig. 9b).

The mafic and ultramafic terrains provide ferromagnesian trace elements, such as Cr and Ni (Hiscott, 1984), while Th is contributed commonly by felsic source (Cullers et al., 1988). Low Th/Cr ratios (0.06) suggest the weathering of mafic and ultramafic sources (McLennan, 2001; Ranjan and Banerjee, 2009). To unravel the degree of weathering Th/U proxy ratios are often used. A decrease a in Th/U ratios suggest an increased weathering and sediments recycling (McLennan and Taylor, 1980;1991; McLennan et al., 1990). In this study the U and Th are slightly enriched compared to UCC. The higher average of Th/U ratio (5.25) as compared to 3.82 in UCC indicates intense weathering conditions prevailing in the source area.

5.5 Geochemistry and provenance

Bhatia (1983) and Roser and Korsch (1986) proposed discrimination diagrams to determine provenance and tectonic settings of the sandstones. The bivariate plots of Bhatia

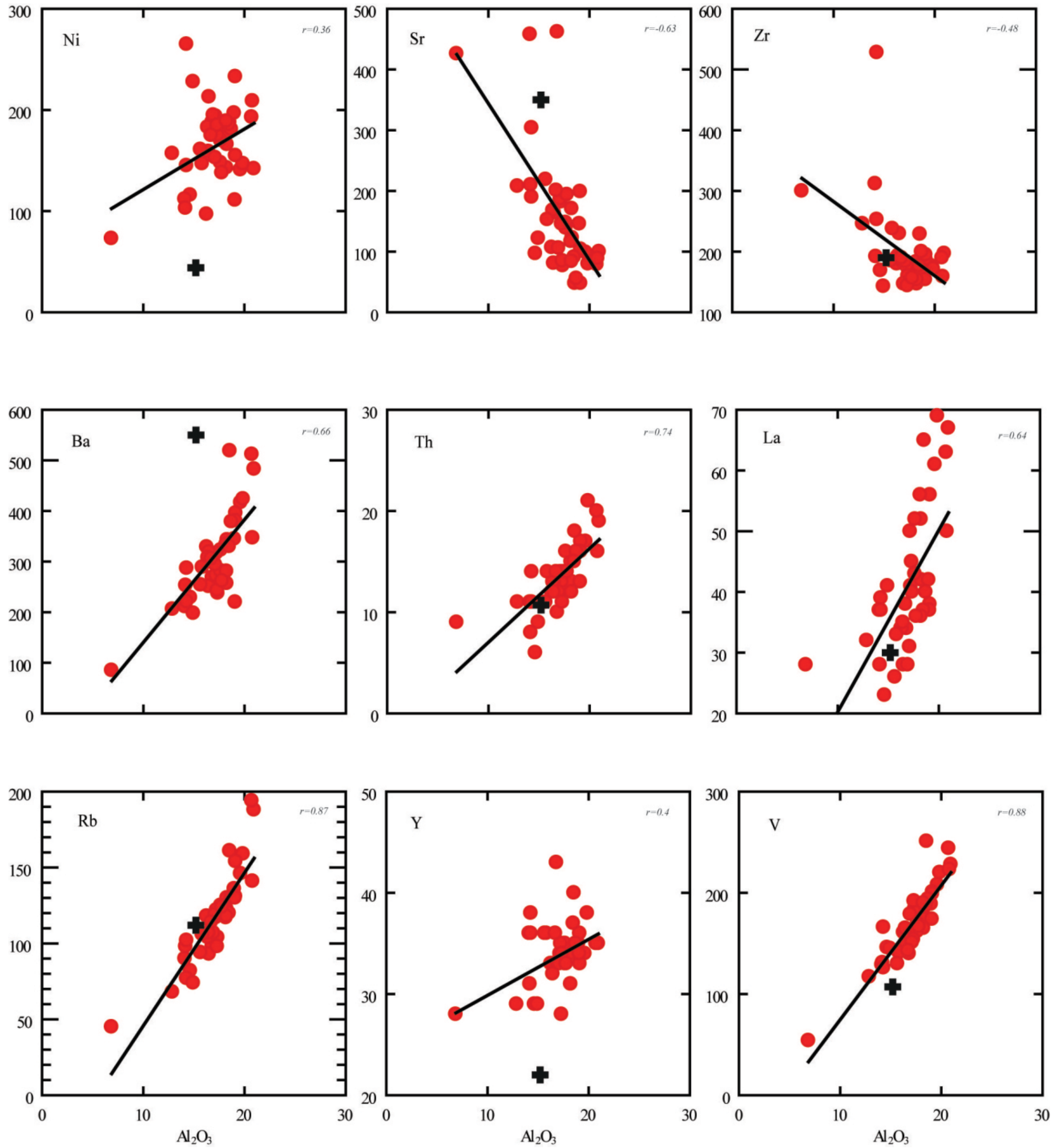

Fig. 8. Variation diagrams of the selected trace elements vs Al_2O_3 of sandstones of the Khojak Formation.

(1983) are divided into different fields such as oceanic arc, continental arc, active continental margin and passive margin (Fig. 10). The Fe_2O_3, MgO and TiO_2 oxides are less mobile and therefore used by Bhatia (1983). The Al_2O_3/SiO_2 ratios provide an estimation of quartz enrichment in sandstones (Bhatia, 1983). In Fe_2O_3+MgO vs TiO_2 bivariate diagram sandstone samples plot inside and very close to the fields of oceanic arc (Fig. 10a), while in Fe_2O_3+MgO vs Al_2O_3/SiO_2 diagram the samples also plot inside and very close to the oceanic arc (Fig. 10b).

A discrimination diagram of Roser and Korsch (1986) correlates SiO_2 vs K_2O/Na_2O (Fig.11) in three fields i.e. island arc, active continental margin and passive margin. In this study majority of the samples plot inside the field of active continental margin while few samples plot beside the boundary of passive margin field within the active continental margin. A couple of samples, however, plot inside the passive margin fields.

Table 3. Major elements concentrations, in weight percentage, and other geochemical parameters for sandstones of the Khojak Formation.

Sections & sample no	SiO_2	TiO_2	Al_2O_3	$Fe_2O_3^{[Total]}$	MnO	MgO	CaO	Na_2O	K_2O	P_2O_5	Sum
LJ-1B	68.74	0.64	14.65	6.51	0.03	4.04	1.08	2.25	1.91	0.15	100
LJ-3B	66.91	0.80	16.27	6.39	0.11	3.71	1.11	1.79	2.72	0.19	100
LJ-6B	69.53	0.79	14.13	6.22	0.14	3.82	1.37	1.51	2.30	0.18	100
LJ-8B	70.06	0.79	14.19	6.15	0.06	3.37	1.16	1.70	2.36	0.16	100
MB-2	62.71	1.01	19.62	8.75	0.07	2.88	1.04	0.77	3.02	0.13	100
MB-3	62.98	0.90	18.28	7.77	0.13	4.38	1.14	1.42	2.86	0.15	100
MB-5	62.82	0.96	19.86	7.86	0.06	3.11	1.04	0.98	3.18	0.14	100
MB-6	64.13	1.01	19.13	7.74	0.12	2.81	1.07	0.86	3.04	0.11	100
MB-7	63.24	0.93	18.17	9.18	0.07	3.49	1.07	1.13	2.50	0.21	100
MB-8	61.75	1.12	20.95	7.49	0.08	3.00	1.06	0.78	3.66	0.11	100
MB-14	64.37	1.27	18.55	7.82	0.02	2.79	1.05	0.50	3.54	0.09	100
MB-15	62.51	1.08	20.73	7.01	0.03	3.03	1.04	0.81	3.64	0.10	100
MB-17	61.32	0.92	18.99	8.43	0.11	4.53	1.14	1.32	3.08	0.17	100
MB-20	67.49	0.85	14.29	9.63	0.18	3.87	1.24	0.42	1.95	0.07	100
MB-21	62.05	0.80	18.24	8.14	0.13	4.96	1.22	1.39	2.89	0.18	100
GHR-1	64.07	0.91	17.66	7.93	0.10	3.93	1.16	1.23	2.85	0.16	100
GHR-3	63.99	0.86	16.82	7.85	0.16	4.79	1.31	1.63	2.42	0.17	100
GHR-4	63.38	0.88	17.17	7.89	0.13	5.09	1.22	1.35	2.73	0.17	100
GHR-8	63.88	0.84	17.64	7.48	0.13	4.34	1.17	1.50	2.83	0.18	100
GHR-11	64.28	0.88	17.24	7.71	0.09	4.27	1.20	1.34	2.83	0.17	100
GHR-14	64.03	0.91	16.51	8.31	0.11	4.95	1.17	1.58	2.24	0.20	100
SPS-1 B	61.61	1.01	19.11	8.18	0.07	4.55	1.05	1.31	2.93	0.19	100
SPS-3	71.89	0.74	12.88	6.57	0.12	3.06	1.18	1.92	1.48	0.15	100
SPS-7B	62.79	1.01	18.70	7.74	0.08	4.13	1.06	1.43	2.86	0.20	100
SPS-9	61.00	0.87	19.08	8.45	0.20	4.58	1.26	0.98	3.37	0.20	100
CH-4	59.11	0.98	20.80	9.08	0.08	4.10	1.06	1.31	3.31	0.17	100
CH-5B	64.84	0.89	17.36	8.17	0.12	3.36	1.06	1.67	2.38	0.17	100
CH-6	65.90	0.80	14.94	8.41	0.19	4.69	1.13	2.13	1.66	0.16	100
CH-7	65.80	0.89	16.38	7.77	0.13	3.89	1.17	1.41	2.40	0.16	100
CH-8B	62.45	0.96	18.48	8.31	0.11	4.03	1.09	1.55	2.82	0.19	100
CH-9B	64.21	0.85	16.94	8.07	0.12	4.61	1.09	1.54	2.40	0.16	100
CH-10A	68.55	0.87	16.46	6.08	0.07	2.47	1.05	2.08	2.23	0.14	100
CH-12	64.20	0.84	17.31	8.61	0.09	3.97	1.05	1.53	2.24	0.16	100
CH-14	63.20	0.90	18.22	8.46	0.11	3.87	1.06	1.36	2.67	0.15	100
CH-15	84.31	0.45	6.87	3.61	0.11	1.41	1.36	1.14	0.68	0.07	100
TTS-1	67.25	0.87	15.83	6.85	0.09	3.83	1.16	1.57	2.38	0.16	100
TTS-7	64.58	0.89	17.12	7.45	0.10	4.34	1.19	1.50	2.66	0.18	100
TTS-14	63.13	0.85	17.78	7.75	0.12	4.90	1.19	1.34	2.77	0.17	100
TTS-16	66.44	0.80	15.67	7.70	0.14	4.15	1.23	1.55	2.15	0.16	100
TTS-21	64.68	0.93	16.71	7.73	0.12	4.52	1.24	1.28	2.62	0.17	100
TTS-28	68.96	0.87	14.29	6.58	0.09	4.13	1.23	1.42	2.27	0.17	100
Mean	**65.10**	**0.89**	**17.07**	**7.66**	**0.10**	**3.90**	**1.15**	**1.37**	**2.61**	**0.16**	**100**
Maximum	84.31	1.27	20.95	9.63	0.20	5.09	1.37	2.25	3.66	0.21	100
Minimum	59.11	0.45	6.87	3.61	0.02	1.41	1.04	0.42	0.68	0.07	100
UCC	**66**	**0.68**	**15.2**	**5.03**	**0.08**	**2.2**	**4.2**	**3.9**	**3.4**	**0.15**	

Sample No.	SiO_2/Al_2O_3	K_2O/Na_2O	TiO_2/Al_2O_3	Fe2O3 +MgO	K2O/Al2O3	CIA	CIW	ICV	CPA
LJ-1B	4.69	0.85	0.04	10.55	0.13	73.69	81.50	15.86	86.69
LJ-3B	4.11	1.52	0.05	10.10	0.17	74.34	84.89	15.87	90.10
LJ-6B	4.92	1.53	0.06	10.05	0.16	73.17	83.08	15.43	90.36
LJ-8B	4.94	1.39	0.06	9.51	0.17	73.11	83.23	14.85	89.29
MB-2	3.20	3.93	0.05	11.63	0.15	80.25	91.57	16.58	96.23
MB-3	3.45	2.01	0.05	12.15	0.16	77.12	87.70	17.75	92.77
MB-5	3.16	3.24	0.05	10.97	0.16	79.24	90.76	16.27	95.30
MB-6	3.35	3.55	0.05	10.54	0.16	79.37	90.84	15.68	95.71
MB-7	3.48	2.22	0.05	12.68	0.14	79.47	89.21	17.49	94.17
MB-8	2.95	4.66	0.05	10.49	0.17	79.20	91.91	16.13	96.39
MB-14	3.47	7.04	0.07	10.60	0.19	78.47	92.29	15.79	97.36
MB-15	3.02	4.47	0.05	10.04	0.18	79.05	91.78	15.62	96.22
MB-17	3.23	2.34	0.05	12.95	0.16	77.42	88.55	18.65	93.51
MB-20	4.72	4.65	0.06	13.50	0.14	79.83	89.61	17.35	97.14
MB-21	3.40	2.08	0.04	13.10	0.16	76.85	87.49	18.77	92.92
GHR-1	3.63	2.31	0.05	11.86	0.16	77.13	88.07	17.25	93.48
GHR-3	3.80	1.48	0.05	12.63	0.14	75.83	85.11	18.21	91.14
GHR-4	3.69	2.03	0.05	12.97	0.16	76.43	86.99	18.45	92.73
GHR-8	3.62	1.89	0.05	11.82	0.16	76.23	86.86	17.50	92.17
GHR-11	3.73	2.12	0.05	11.98	0.16	76.26	87.18	17.48	92.79
GHR-14	3.88	1.42	0.06	13.26	0.14	76.79	85.74	18.41	91.28
SPS-1 B	3.22	2.23	0.05	12.73	0.15	78.32	89.00	18.14	93.58
SPS-3	5.58	0.77	0.06	9.63	0.12	73.77	80.62	14.39	87.03
SPS-7B	3.36	2.01	0.05	11.87	0.15	77.78	88.29	17.35	92.92
SPS-9	3.20	3.42	0.05	13.03	0.18	77.26	89.47	18.90	95.09
CH-4	2.84	2.54	0.05	13.18	0.16	78.56	89.78	18.99	94.10
CH-5B	3.73	1.43	0.05	11.52	0.14	77.27	86.44	16.80	91.24
CH-6	4.41	0.78	0.05	13.10	0.11	75.24	82.09	18.26	87.52
CH-7	4.02	1.70	0.05	11.66	0.15	76.67	86.39	16.83	92.06
CH-8B	3.38	1.82	0.05	12.34	0.15	77.16	87.47	17.97	92.24
CH-9B	3.79	1.55	0.05	12.68	0.14	77.10	86.54	17.88	91.66
CH-10A	4.17	1.07	0.05	8.55	0.14	75.42	84.00	14.03	88.77
CH-12	3.71	1.47	0.05	12.58	0.13	78.22	87.04	17.54	91.90
CH-14	3.47	1.96	0.05	12.33	0.15	78.18	88.27	17.58	93.06
CH-15	12.28	0.60	0.07	5.02	0.10	68.38	73.33	8.37	85.76
TTS-1	4.25	1.51	0.06	10.68	0.15	75.58	85.26	15.94	90.96
TTS-7	3.77	1.78	0.05	11.80	0.16	76.23	86.46	17.28	91.97
TTS-14	3.55	2.07	0.05	12.66	0.16	77.05	87.55	18.12	93.01
TTS-16	4.24	1.39	0.05	11.85	0.14	76.05	84.92	16.98	90.99
TTS-21	3.87	2.05	0.06	12.26	0.16	76.50	86.91	17.57	92.90
TTS-28	4.83	1.60	0.06	10.70	0.16	74.41	84.36	15.77	90.98
Mean	**4.00**	**2.21**	**0.05**	**11.55**	**0.15**	**76.69**	**86.79**	**16.83**	**92.33**
Maximum	12.28	7.04	0.07	13.50	0.19	80.25	92.29	18.99	97.36
Minimum	2.84	0.60	0.04	5.02	0.10	68.38	73.33	8.37	85.76
UCC	**4.34**	**0.87**	**0.04**	**7.23**	**0.22**				

Table 4. Trace elements concentrations, in ppm, and other geochemical parameters for sandstones of the Khojak Formation.

Sample No.	Cr	Ni	Cu	Zn	Sr	Zr	Ba	Ce	Th	Ga	Pb	La	Rb	U	Y	Nb	V
LJ-1B	178	116	31	86	97	169	229	46	6	18	17	23	82	1	29	10	146
LJ-3B	179	97	42	84	107	180	329	70	12	20	23	34	118	4	33	12	161
LJ-6B	284	112	26	84	458	312	211	70	11	19	25	37	90	3	36	14	129
LJ-8B	197	103	30	75	210	192	253	57	8	19	19	28	98	1	31	12	131
MB-2	217	141	33	121	99	177	417	117	17	23	21	61	146	3	34	21	208
MB-3	229	166	40	103	123	165	343	85	15	23	23	42	130	3	34	16	174
MB-5	200	147	38	118	80	172	424	124	21	24	19	69	159	4	38	20	220
MB-6	225	155	29	93	104	188	396	105	17	24	16	56	154	3	33	20	201
MB-7	236	175	29	101	117	183	334	105	15	21	17	56	117	2	34	18	186
MB-8	227	142	37	125	100	197	483	126	19	25	17	67	188	4	35	22	228
MB-14	338	188	43	101	48	229	519	123	18	23	21	65	161	4	40	28	251
MB-15	333	193	44	129	79	190	512	119	20	25	15	63	194	4	35	22	244
MB-17	223	197	43	110	146	164	345	83	16	23	18	42	136	3	35	15	189
MB-20	1883	265	43	181	304	528	221	78	11	20	48	37	77	4	38	17	166
MB-21	185	143	55	113	171	147	257	95	13	23	19	52	123	4	34	12	165
GHR-1	223	170	37	107	139	174	323	98	16	21	22	52	125	3	35	16	170
GHR-3	254	188	48	161	462	184	269	71	10	21	37	34	98	1	43	14	140
GHR-4	235	194	46	106	182	179	273	93	13	22	23	50	117	4	34	16	153
GHR-8	211	148	36	98	148	160	282	82	14	22	22	43	121	4	33	14	162
GHR-11	241	183	47	105	146	176	317	79	13	22	23	41	122	1	35	16	154
GHR-14	300	213	48	112	164	230	319	57	13	20	22	28	93	2	33	16	151
SPS-1 B	299	233	45	106	48	195	381	73	16	22	19	38	131	4	36	17	199
SPS-3	293	157	37	85	208	246	206	60	11	18	22	32	68	2	29	13	117
SPS-7B	244	181	37	102	56	200	379	79	16	22	13	40	130	4	35	18	194
SPS-9	170	111	49	121	199	154	220	73	13	23	21	37	130	3	34	13	174
CH-4	244	209	53	123	89	159	347	96	16	23	16	50	141	3	35	16	223
CH-5B	276	175	50	99	77	160	238	77	14	20	16	40	104	4	34	15	184
CH-6	268	228	53	106	122	143	198	76	9	19	20	41	74	1	29	14	145
CH-7	265	183	46	102	168	193	308	69	13	21	21	34	104	2	33	16	161
CH-8B	238	186	47	101	91	177	330	77	15	22	15	37	120	4	37	15	187
CH-9B	230	195	47	100	106	147	302	55	12	21	18	28	107	3	33	14	179
CH-10A	382	159	42	76	81	191	251	69	12	20	14	35	107	2	32	13	165
CH-12	251	185	57	104	85	144	243	84	11	20	17	45	98	3	28	14	192
CH-14	265	189	51	100	84	154	281	70	12	21	18	36	118	1	31	15	190
CH-15	365	73	14	56	426	300	85	56	9	15	7	28	45	1	28	11	54
TTS-1	269	147	34	98	153	238	289	68	14	20	26	33	106	3	36	15	141
TTS-7	211	153	46	103	187	184	294	68	14	21	21	31	119	4	33	17	151
TTS-14	181	138	44	103	194	157	262	70	14	21	18	36	124	2	33	13	167
TTS-16	238	161	46	101	219	185	254	58	11	20	27	26	94	1	36	15	130
TTS-21	228	175	50	105	201	190	306	77	14	21	22	38	114	2	36	17	143
TTS-28	254	145	30	89	190	253	287	75	14	20	22	39	102	2	36	17	126
Mean	**287**	**166**	**41**	**105**	**158**	**197**	**305**	**81**	**14**	**21**	**20**	**42**	**117**	**3**	**34**	**16**	**170**
Maximum	1883	265	57	181	462	528	519	126	21	25	48	69	194	4	43	28	251
Minimum	170	73	14	56	48	143	85	46	6	15	7	23	45	1	28	10	54
UCC	**83**	**44**	**25**	**71**	**350**	**190**	**550**	**64**	**10.7**		**17**	**30**	**112**	**2.8**	**22**	**12**	**107**

Sample No.	Th/Cr	Cr/Ni	Cr/V	Y/Ni	Th/U	Cr/Zr	V/Ni
LJ-1B	0.04	1.53	1.21	0.25	6.00	1.05	1.26
LJ-3B	0.07	1.85	1.11	0.34	2.75	0.99	1.67
LJ-6B	0.04	2.52	2.20	0.32	4.00	0.91	1.15
LJ-8B	0.04	1.91	1.50	0.30	7.00	1.02	1.27
MB-2	0.08	1.54	1.05	0.24	5.33	1.23	1.47
MB-3	0.06	1.38	1.31	0.21	4.33	1.39	1.05
MB-5	0.10	1.36	0.91	0.26	5.00	1.16	1.50
MB-6	0.08	1.45	1.12	0.21	5.33	1.20	1.30
MB-7	0.06	1.35	1.26	0.20	7.00	1.29	1.07
MB-8	0.08	1.60	1.00	0.25	4.50	1.15	1.60
MB-14	0.05	1.80	1.35	0.21	4.25	1.47	1.34
MB-15	0.06	1.72	1.36	0.18	4.75	1.75	1.26
MB-17	0.07	1.13	1.18	0.18	4.67	1.36	0.96
MB-20	0.01	7.12	11.37	0.14	3.00	3.57	0.63
MB-21	0.07	1.30	1.13	0.24	3.67	1.26	1.15
GHR-1	0.07	1.32	1.32	0.21	4.67	1.28	1.00
GHR-3	0.04	1.35	1.81	0.23	8.00	1.38	0.74
GHR-4	0.06	1.21	1.54	0.18	3.67	1.32	0.79
GHR-8	0.07	1.43	1.30	0.22	4.00	1.31	1.10
GHR-11	0.05	1.32	1.57	0.19	11.00	1.37	0.84
GHR-14	0.04	1.41	1.99	0.15	5.50	1.30	0.71
SPS-1 B	0.05	1.28	1.50	0.15	3.75	1.53	0.86
SPS-3	0.04	1.87	2.52	0.19	4.50	1.19	0.74
SPS-7B	0.06	1.35	1.26	0.19	3.75	1.22	1.08
SPS-9	0.07	1.53	0.98	0.31	5.00	1.11	1.57
CH-4	0.07	1.17	1.10	0.17	5.00	1.53	1.07
CH-5B	0.05	1.58	1.51	0.19	3.25	1.72	1.05
CH-6	0.03	1.18	1.84	0.13	8.00	1.87	0.64
CH-7	0.05	1.45	1.64	0.18	5.50	1.38	0.88
CH-8B	0.06	1.28	1.27	0.20	3.50	1.35	1.01
CH-9B	0.05	1.18	1.28	0.17	3.67	1.57	0.92
CH-10A	0.03	2.40	2.31	0.20	5.50	1.99	1.04
CH-12	0.04	1.35	1.31	0.15	3.33	1.74	1.03
CH-14	0.04	1.40	1.40	0.16	11.00	1.72	1.01
CH-15	0.03	4.98	6.73	0.39	7.00	1.22	0.74
TTS-1	0.05	1.83	1.91	0.25	4.00	1.13	0.96
TTS-7	0.07	1.38	1.40	0.22	4.00	1.15	0.98
TTS-14	0.08	1.31	1.09	0.24	6.00	1.15	1.21
TTS-16	0.05	1.47	1.82	0.22	9.00	1.29	0.81
TTS-21	0.06	1.30	1.60	0.21	5.50	1.20	0.82
TTS-28	0.05	1.75	2.02	0.25	5.50	1.00	0.86
Mean	**0.06**	**1.72**	**1.83**	**0.22**	**5.25**	**1.39**	**1.05**
Maximum	0.10	7.12	11.37	0.39	11.00	3.57	1.67
Minimum	0.01	1.13	0.91	0.13	2.75	0.91	0.63
UCC	**0.13**	**1.89**	**0.78**	**0.5**	**3.82**	**0.44**	**2.43**

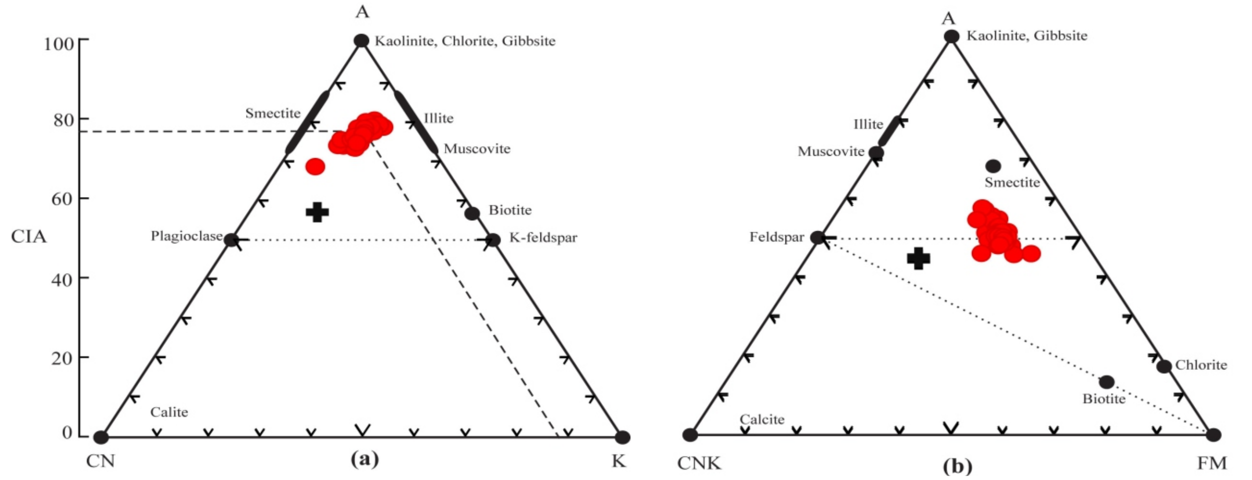

Fig. 9. (a) A-CN-K and CIA plots (after Nesbitt and Young, 1982, Nesbitt et al., 1996) for sandstones of the Khojak Formation; (b) ACNK-FM plots (after Nesbitt et al., 1996) for the sandstones of the Khojak Formation; A = Al_2O_3, CN = CaO + Na_2O, K = K_2O, CNK = CaO +Na_2O + K_2O, FM = Fe_2O_3+MgO

Ratios of oxides such as Ti, Fe, Mg, Na and K with Al_2O_3 can be used to determine the provenance of the sandstone-mudstone suites. Roser and Korsch (1988) proposed such a diagram divided into four fields of provenance i.e. quartzose sedimentary, felsic igneous, intermediate igneous and mafic igneous (Fig. 12). The majority of the sandstone samples plot inside the quartzose sedimentary provenance, however very close to the junction of mafic and intermediate igneous provenance (Fig. 12).

Trace elements have also been used to determine provenance. The high Field Strength Elements such as Zr, Nb, Y, Th and U are immobile hence useful in provenance studies (see e.g. Taylor and McLennan, 1985). In sandstones of Khojak Formation Zr, Nb, Y, Th and U are marginally enriched compared to UCC (Table 3), which suggest contribution from felsic sources. The ultramafic suites, by contrast largely provide Cr and Ni, while V is derived from mafic sources (e.g. Hiscott, 1984; Feng and Kerrich, 1990; McLennan, 2001). The Cr is a reliable tracer for ophiolitic rocks (Hiscott, 1978). The concentrations of Cr and Ni are high (Table 3), moderate ratios of Cr/Ni (1.72) and Cr/V (1.83) suggest contributions from the mafic and ultramafic sources. The Th/Cr ratios average to 0.06 and range from 0.01 to 0.10, which is highly depleted compared to UCC (0.13). Th/Cr ratios ranging from 0.13 to 2.7 indicate felsic suites and ratios ranging from 0.018 to 0.046 are typical of mafic suites (Cullers, 2000). The Cr/Zr ratio in the Khojak sandstones averages to 1.39 and ranges from 0.91 to 3.57 (UCC average: 0.44; Table 3). The high Cr/Zr and Th/Cr ratio indicate contribution from mafic rocks (e.g. Wronkiewicz and Condie, 1988; McLennan et al., 1993; Garver et al., 1996; Bock et al., 1998; Armstrong-Altrin et al., 2004; Meinhold et al., 2007 and Rahman and Suzuki, 2007). The sandstones formed as results of Ophiolite source have high concentrations of Cr in relation to over other ferromagnesian elements (see e.g. Garver et al., 1996). This results in higher Cr/V and low Y/Ni ratios. The Cr enrichment in such sandstone is probably due to the Chromite in ophiolites suite (e.g. Hiscott, 1984), while Ni is enriched as a result of orthopyroxenes breakdown into pyrite (Bock et al., 1998).

6. Discussion

Petrologically the Khojak sandstone is meta-sedimentary litharenite (Qayyum et al., 2001) and has been derived from recycled orogen. The higher percentages of the lithic fragments further cause the sandstone samples to plot in the transitional recycled provenance in QmFLt plot (Fig. 4) (Qayyum et al., 2001). The sediments dispersal pattern and palaeocurrent directions to the southwest suggest that the steadily uplifting Himalayan orogenic belt, was the main source terrain for the Khojak sediments (Qayyum, et al., 1996, 1997). Up-section the overall decrease in the percentage of monocrystalline quartz and increase in total lithic and metamorphic fragments reflects the gradual erosion of Himalayas to its deeper parts (Qayyum et al., 2001). Increase of volcanic lithic fragments up section shows increasing contribution from suture zone of the Kohistan Island Arc (Qayyum et al., 2001). However, due to the

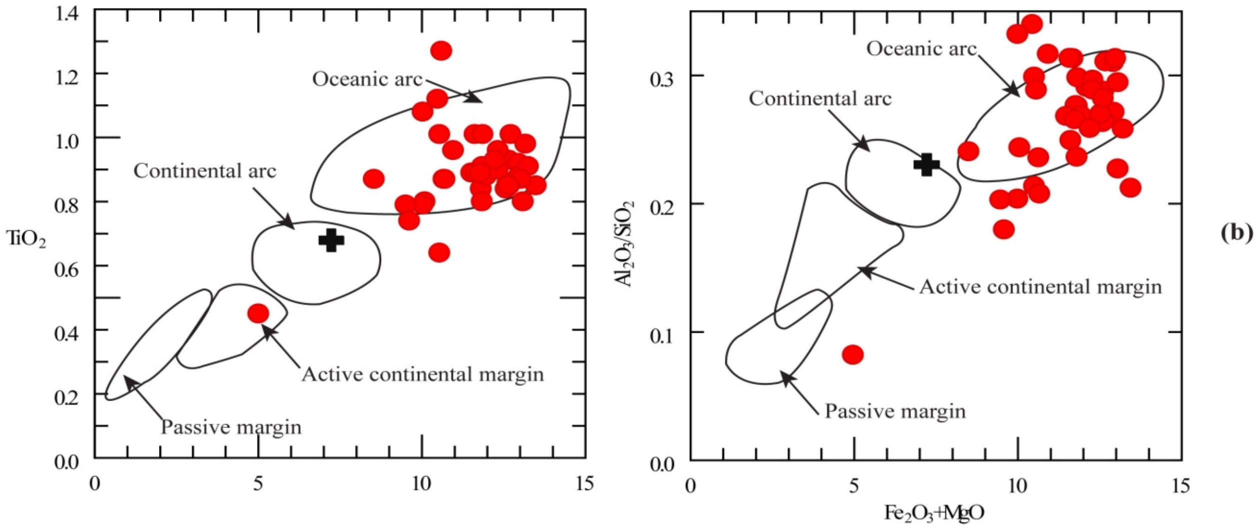

Fig. 10. Tectonic discrimination diagrams (after Bhatia, 1983) for sandstone samples of the Khojak Formation; (a) Fe_2O_3+MgO vs TiO_2 and (b) Fe_2O_3+MgO vs Al_2O_3/SiO_2.

proximity of the outcrops to the Katawaz Basin, a substantial contribution from the Zhob-Waziristan and Bela-Muslim Bagh Ophiolite in Kirthar-Sulaiman Fold-Thrust Belt cannot be ignored. The U-Pb dating of zircon in the Khojak sandstone also supports the Himalayan source for the siliciclastic detritus of Katawaz basin (Carter et al., 2010). Carter et al. (2010) believe that zircon grains of the Cretaceous-Paleocene age have been shed from magmatic arc and basement rocks of either Indian Plate or Eurasian Plate (Karakoram block).

The major and trace elements geochemistry confirms that the Himalayan collision zone was the most probable source of sedimentary shed which has contributed to the sandstones of the Katawaz Delta and Khojak-Panjgur Submarine Fan (Qayyum et al., 1996a, 1996b, 1997a, 1997b). The plots in this study suggest that the Sulaiman and Kirthar Fold–Thrust Belts, Ophiolitic complexes of Muslim Bagh, Zhob and Waziristan have significantly provided the detritus to the Katawaz Delta. The geochemical data proposes felsic detritus from the Himalayan orogen and mafic/ultramafic detritus from the Muslim Bagh-Waziristan Ophiolite. Initially, low- to high-grade metamorphic and granitic sediments were carried from the Himalaya and Kohistan Island Arc, however in later stages onset of detritus shed the mafic/ultramafic suites of the Sulaiman Fold-Thrust Belt and Muslim Bagh-Zhob-Waziristan Ophiolite was prevalent (see e.g. Allemann, 1979; Beck et al., 1995; Garzanti et al., 1996; Qayyum et al., 1996a, 1996b, 1997a, 1997b). The trace element ratios such as of Cr/V, V/Ni, Cr/Ni and Y/Ni, clearly indicate contribution from mafic/ultramafic suite.

The Khojak Formation is a river dominated and wave modified delta-submarine fan system. During the Oligocene and Miocene the Katawaz remnant ocean was the main depo-center for Himalayan detritus (Qayyum et al., 1997a; 1997b; Clift et al., 2001; Kassi et al., 2011; 2015). Over the course of time proto-Indus river changes its course in such a way that presently only the Himalayan sediments started to feed the present Indus Delta and associated submarine fan in Indian ocean (Davies et al., 1995; Qayyum et al., 1997a, b). The deltaic sandstone of the Khojak Formation, turbidite succession of the Panjgur Formation and molasse strata of the Muree Formation (Himalayan forelands) have recorded outstandingly similar detrital modes (Critelli and De Rosa, 1987; Critelli et al., 1990; Critelli and Garzanti, 1994; Qayyum et al., 2001; Clift et al., 2001; Najman, 2006; Kassi et al., 2015). The Qt–F–L modes of sandstone of Khojak (Qt60–F9–L31), Muree (Qt66–F8–L26) and Panjgur formations (Qt56–F11–L33 of Critelli et al., 1990 and Qt65–F10–L26 of Kassi et al., 2015) are closely comparable. During Paleogene, in the Himalayas, only sedimentary and metasedimentary rocks were exposed while the high-grade metamorphic rocks started contributing their detritus in later stage. The Katawaz delta and associated Khojak submarine-fan system started depositing in the Katawaz remnant ocean that has opened

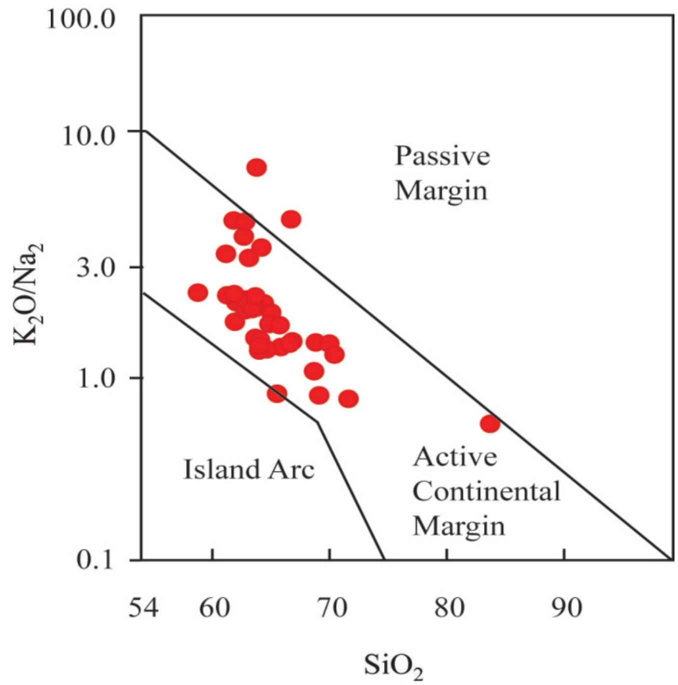

Fig. 11. Bivariate plot of (K2O/Na2O) vs. SiO2 (after Roser and Korsch, 1986) for discrimination of the tectonic settings of sandstones of the Khojak Formation.

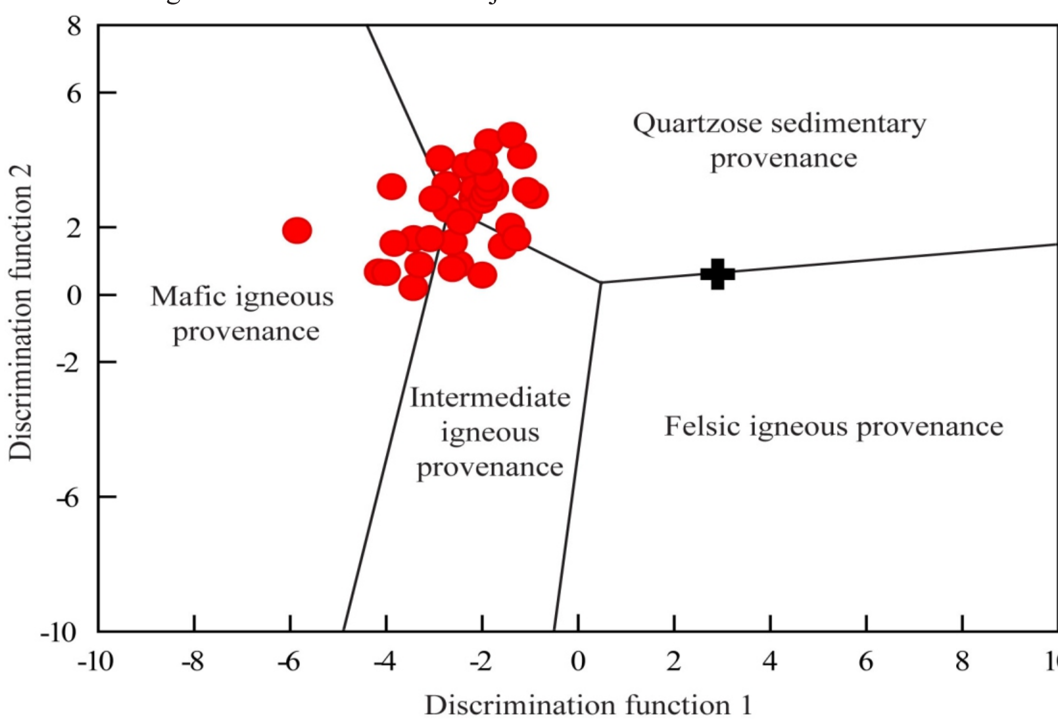

Fig, 12. Discrimination function diagram (after Roser and Korsch, 1988) for the sandstone of Khojak Formation.

between the Afghan block and northwestern margin of the Indian Plate subsequent to the closure of Neo Tethys. Succession of the Katawaz Basin or Pishin belt is bounded by the Ornach-Nushki-Chaman fault in the west and by Zhob valley thrust in the east. The west-northwest-dipping Zhob valley thrust brings the highly deformed succession of the Katawaz Basin on top of the Muslim Bagh Ophiolite and associated mélanges.

7. Conclusions

According to the Herron's (1988) classification scheme the sandstone samples plot inside the shale/wacke field close to Fe-shale field while in the Pettijohn's (1987) scheme the samples fall on the boundary between greywacke and litharenite field. Both of the classifications show that higher K_2O and Al_2O_3 contents control the distribution of sandstone samples in the classification scheme. The geochemistry of wacke to litharenite supports the petrographic data. Similar SiO_2/Al_2O_3 ratios compared to UCC reflect the moderately mature nature of the sandstones, due to quartz enrichment. The higher K_2O/Na_2O ratios relative to UCC, reflect dominance of the Alkali feldspars over plagioclase. Fairly high mean percentages of Fe_2O_3 and MgO as compared to UCC and constant ratios of TiO_2/Al_2O_3 is attributed to the higher proportion of ferromagnesian minerals derived from mafic and ultramafic rocks. The trace element analyses indicate that Zr and Rb are slightly enriched while Cr, Ni and V are highly enriched as compared to UCC values, which attest to the substantial contribution from local mafic and ultramafic detritus.

The CIA values for sandstones (mean ~77) indicates moderate to strong degree of weathering. Similarly CIW values (mean ~87) indicate moderately to very strongly weathered source terrain. Again CPA values of the sandstones (mean ~92) indicate very strong weathering at source terrain. The high Th/U ratios (5.25) also suggest intense weathering of the source terrain.

The petrographic and geochemical data support the theory that the sediments of the Khojak Formation were mostly derived from the Himalayan Belt, associated suture belts, Kohistan magmatic arc and ophiolite belt.

Detrital modes of the Khojak Formation are highly comparable with turbiditic Panjgur and fluvial Murree formations, which are all part of the same system. This study support the Katawaz delta–Khojak–Panjgur submarine-fan model and that the south-southwest ward transport of Himalayan detritus was being controlled by the Chaman transform fault. However, the tributaries from east were also carrying material from largely mafic Muslim Bagh-Zhob Ophiolite.

References

Allemann, F., 1979. Time of Emplacement of the Zhob Valley Ophiolites and Bela Ophiolites, Baluchistan (Preliminary Report). In: Farah, A., DeJong, K.A. (Eds.), Geodynamics of Pakistan. Geological Survey of Pakistan, Quetta, 215-242.

Armstrong-Altrin, J.S., Lee, Y.H., Verma, S.P., Ramasamy, S., 2004. Geochemistry of sandstones from the upper Miocene Kudankulam Formation, Southern India: implications for provenance, weathering, and tectonic setting. Journal of Sedimentary Research, 74, 285-297.

Basu, A., 1985. Influence of climatic and relief on compositions of sands released at source areas. In: Zuffa, G.G. (Ed.), Provenance of Arenites. NATO, Advanced Study Institute Series, 148, 1-18.

Beck, R.A., Burbank, D.W., Sercombe, W.J., Riley, G.W., Barndt, J.K., Berry, J.R., Afzal, J., Khan, A.M., Jurgen, H., Metjee, J., Cheema, A., Shafique, N.A., Lawrence, R.D., Khan, M.A., 1995. Stratigraphic evidence for an early collision between northeast India and Asia. Nature, 373, 55–58.

Bender, F.K., Raza, H.A., 1995. Geology of Pakistan. Gebrüder Bornträger, Germany.

Bhatia, M.R, 1983, Plate tectonics and geochemical composition of sandstones. The Journal of Geology, 9, 611-627.

Bock, B., McLennan, S.M., Hanson, G.N., 1998. Geochemistry and provenance of the Middle Ordovician Austin Glen Member (Normanskill Formation) and the Taconian Orogeny in New England. Sedimentology, 45, 635–655.

Buggle, B., Glaser, B., Hambach, U., Gerasimenko, N., Markovic, S., 2011. An evaluation of geochemical weathering indices in loessepaleosol studies. Quaternary International, 240, 12-21.

Carter, A., Najman, Y., Bahroudi, A., Bown, P., Garzanti, E., Lawrence, R.D., 2010. Locating earliest records of orogenesis in western Himalaya: evidence from Paleogene sediments in the Iranian Makran region and Pakistan Katawaz basin. Geology, 38, 807–810.

Clift, P.D.N., Shimizu, N.G., Layne, G.C., Gaedicke, C.H.U., Schlüter, H.U.M., Clark, M., Amjad, S., 2001. Development of the Indus Fan and its significance for the erosional history of the western Himalaya and Karakoram. Geological Society of America Bulletin, 113, 1039-1051.

Cox, R., Lowe, D.R., Cullers, R.L., 1995. The influence of sediment recycling and basement composition on evolution of mudrock chemistry in the southwestern United States. Geochimica et Cosmochimica Acta, 59, 2919-2940.

Critelli, S., De Rosa, R., 1987. Composizione e provenienza della arenite oligomioceniche della Formazione di Panjgur (Catena del Makran), Pakistan. G. Geol. 49, 187-196.

Critelli, S., Rosa, R.D., Platt, J.P., 1990. Sandstone detrital modes in the Makran accretionary wedge, southwest Pakistan: Implications for tectonic setting and long-distance turbidite transportation. Sedimentary Geology, 68, 241-260.

Critelli, S., Garzanti, E., 1994. Provenance of the Lower Tertiary Murree redbeds (Hazara-Kashmir syntaxis) and initial rising of the Himalayas. Sedimentary Geology, 89, 265-284.

Cullers, R.L., 2000. The geochemistry of shales, siltstones and sandstones of Pennsylvanian-Permian age, Colorado, USA: implications for provenance and metamorphic studies. Lithos, 51, 181-203.

Cullers, R.L., Basu, A., Suttner, L., 1988. Geochemical signature of provenance in sand-size material in soils and stream sediments near the Tobacco Root batholith, Montana, USA. Chemical Geology, 70, 335-348.

Davies, T.A., Kidd, R.B., Ramsay, A.T.S., 1995. A time-slice approach to the history of Cenozoic sedimentation in the Indian Ocean. Sedimentary Geology, 96, 157-179.

Dickinson, W.R., Suczek, C.A., 1979. Plate Tectonics and Sandstone Composition. American Association of Petroleum Geologists Bulletin, 63, 2164-2182.

Dickinson, W.R., Beard, L.S., Brakenridge, G.R., Erjavec, J.L., Ferguson, R.C., Inman, K.F., Kneep, R.A., Lindberg, F.A., Ryberg, P.T., 1983. Provenance of North America Phanerozoic sandstones in relation to tectonic setting. Geological Society of America Bulletin, 94, 222-235.

Fedo, C. M., Nesbitt, H.W., Young, G.M., 1995. Unraveling the effects of potassium metasomatism in sedimentary rocks and paleosols, with implications for paleoweathering conditions and provenance. Geology, 23, 921-24.

Feng, R., Kerrich, R., 1990. Geochemistry of fine-grained clastic sediments in the Archean Abitibi greenstone belt, Canada: Implications for provenance and tectonic setting. Geochimica et Cosmochimica Acta, 54, 1061-1081.

Garver, J.I., Royce, P.R., Smick, T.A., 1996. Chromium and nickel in shale of the Taconic Foreland: a case study for the provenance of fine-grained sediments with an ultramafic source. Journal of Sedimentary Research, 66, 100-106.

Garzanti, E., Critelli, S., Ingersoll, R.V., 1996. Paleogeography and paleotectonic evolution of the Himalayan Range as reflected by detrital modes of Tertiary sandstones and modern sands (Indus transect, India and Pakistan). Geological Society of America Bulletin, 108, 631-642.

Graham, S.A., Dickinson, W.R., Ingersoll, R.V., 1975. Himalayan-Bengal model for flysch dispersal in the Appalachian-Ouachita System: Geological Society of America Bulletin, 86, 273-286.

Harker, A., 1909. The natural history of igneous rocks. Macmillan Publisher, New York.

Harnois L., 1988. The CIW Index: A New Chemical Index of Weathering. Sedimentary Geology, 55, 319-322.

Herron, M.M., 1988. Geochemical classification of terrigenous sands and shales from core or log data. Journal of Sedimentary Research, 58, 820–829.

Hiscott, R.N., 1978. Provenance of Ordovician deep-water sandstones, Tourelle Formation, Quebec, and implications for initiation of the Taconic orogeny. Canadian Journal of Earth Science, 15, 1579-1597.

Hiscott, R.N., 1984. Ophiolitic source rocks for

Taconic-age Flysch: Trace-element evidence. Geological Society of America Bulletin, 95, 1261-1267.
Ingersoll, R.V., Suczek, C.A., 1979. Petrology and provenance of Neogene sand from Nicobar and Bengal Fans, DSDP sites 211 and 218. Journal of Sedimentary Research, 49, 1217-1228.
Ingersoll, R.V., Bullard, T.F., Ford, R.L., Grimm, J.P., Pickle, J.D., Sares, S.W., 1984. The effect of grain size on detrital modes: A test of the Gazzi-Dickinson point-counting method. Journal of Sedimentary Research, 54, 103-116.
Iqbal, M., 2004. Integration of Satellite Data and Field Observation in Pishin Basin, Balochistan. Pakistan Journal of Hydrocarbon Research, 14, 1-17.
Iqbal, M.W.A., Shah, S.M.I., 1980. A guide to the stratigraphy of Pakistan. Geological Survey of Pakistan, Quetta.
Jadoon, I.A.K., Khurshid, A., 1996. Gravity and tectonic model across the Sulaiman fold belt and the Chaman fault zone in western Pakistan and eastern Afghanistan. Tectonophysics, 254, 89-109.
Jones, A.G., 1961. Reconnaissance geology of part of West Pakistan. A Colombo Plan Cooperative Project, Govt. of Canada, Toronto.
Kasi, A.K., Kassi, A.M., Umar, M., Manan, R.A., Kakar, M.I., 2012. Revised lithostratigraphy of the Pishin Belt, northwestern Pakistan. Journal of Himalayan Earth Sciences, 45, 53-65.
Kassi, A.M., Khan, A.S., Kelling, G., Kasi, A.K., 2011. Facies and cyclicity within the Oligocene-Early Miocene Panjgur Formation, Khojak–Panjgur Submarine Fan Complex, south-west Makran, Pakistan. Journal of Asian Earth Sciences, 41, 537-550.
Kassi, A.M., Grigsby, J.D., Khan, A.S., Kasi, A.K., 2015. Sandstone petrology and geochemistry of the Oligocene–Early Miocene Panjgur Formation, Makran accretionary wedge, southwest Pakistan: Implications for provenance, weathering and tectonic setting. Journal of Asian Earth Sciences, 105, 192-207.
Kazmi, A.H., Jan, M.Q., 1997. Geology and Tectonics of Pakistan. Graphic Publishers, Karachi.
Klootwijk, C.T., Gee, J.S., Peirce, J.W., Smith, G.M., McFadden, P.L., 1992. An early India-Asia contact: Paleomagnetic constraints from Ninety East Ridge, ODP Leg 121. Geology, 20, 395-398.
Lawrence, R.D., Yeats, R. S., 1979. Geological Reconnaissance of Chaman Fault in Pakistan. In: Farah, A., DeJong, K.A., (Eds.), Geodynamics of Pakistan. Geological Survey of Pakistan, Quetta, 351-357.
Lawrence, R.D., Khan, S.H., DeJong, K.A., Farah, A., Yeats, R.S., 1981. Thrust and strike slip fault interaction along the Chaman transform zone, Pakistan. In: McClay, K., Price, N.J. (Eds.), Thrust and Nappe Tectonics. Geological Society of London, Special Publication 9, 363-370.
McCall, G.J.H., Kidd, R.G.W., 1982. The Makran, southeastern Iran: the anatomy of a convergent plate margin active from Cretaceous to Present. In: Leggett, J.K. (Ed.), Trench-Forearc Geology. Geological Society of London, Special Publication, 10, 387–397.
McLennan, S.M., 2001. Relationships between the trace element composition of sedimentary rocks and upper continental crust. Geochemistry Geophysics Geosystems, 2, (4).
McLennan, S.M., Taylor, S.R., 1980. Th and U in sedimentary rocks: crustal evolution and sedimentary recycling. Nature, 285, 621-624.
McLennan, S.M., Taylor, S.R., 1991. Sedimentary rocks and crustal evolution: tectonic setting and secular trends. The Journal of Geology, 99, 1-21.
McLennan, S.M., Taylor, S.R., McColloch, M.T., Maynard, J.B., 1990. Geochemical and Nd–Sr isotopic composition of deep sea turbidites: crustal evolution and plate tectonic association. Geochimica et Cosmochimica Acta, 54, 2015-2050.
McLennan, S.M., Hemming, S., McDaniel, D.K., Hanson, G.N., 1993. Geochemical approaches to sedimentation, provenance and tectonics. Geological Society of

America, special paper, 284.
Meinhold, G., Kostopoulos, D., Reischmann, T., 2007. Geochemical constraints on the provenance and depositional setting of sedimentary rocks from the islands of Chios, Inousses and Psara, Aegean Sea, Greece: implications for the evolution of Paleotethys. Journal of Geological Society of London, 164, 1145-1163.
Najman, Y., 2006. The detrital record of orogenesis: a review of approaches and techniques used in the Himalayan sedimentary basins. Earth Science Review, 74, 1-72.
Nesbitt, H.W., Young, G.M., 1982. Early Proterozoic climates and plate motions inferred from major element chemistry of lutites. Nature, 299, 715-717.
Nesbitt, H.W., Young, G.M., 1984. Prediction of some weathering trends of plutonic and volcanic rocks based on thermodynamic and kinetic considerations. Geochimica et Cosmochimica Acta, 48, 1523-1534.
Nesbitt, H.W., Young, G.M., McLennan, S.M., Keays, R.R., 1996. Effects of chemical weathering and sorting on the petrogenesis of siliciclastic sediments, with implications for provenance studies. Journal of Geology, 104, 525-542.
Pettijohn, F.J., Potter, P.E., Siever, R., 1987. Sand and Sandstone. Springer-Verlag, New York.
Platt, J.P., Leggett, J.K., 1986. Stratal extension in thrusts of footwalls, Makran accretionary prism, implications for thrust tectonics. American Association of Petroleum Geologists Bulletin, 70, 191-203.
Powell, C.M.A., 1979. A Speculative Tectonic History of Pakistan and Surroundings: Some Constraints from the Indian Ocean. In: Farah, A., DeJong, K.A. (Eds.), Geodynamics of Pakistan. Geological Survey of Pakistan, Quetta, 5-24.
Qayyum, M., Niem, A.R., Lawrence, R.D., 1996. Newly discovered Paleogene deltaic sequence in Katawaz basin, Pakistan and its tectonic implications. Geology, 24, 835-838.
Qayyum, M., Lawrence, R.D., Niem, A.R., 1997a. Molasse-delta continuum of the Himalayan orogeny and closure of the Paleogene Katawaz remnant ocean, Pakistan. International Geology Review, 39, 861–875.
Qayyum, M., Lawrence, R.D., Niem, A.R., 1997b. Discovery of the paleo-Indus delta fan complex. Geol. Soc. London J. 154, 753–756.
Qayyum, M., Niem, A.R., Lawrence, R.D., 2001. Detrital modes and provenance of the Paleogene Khojak Formation in Pakistan: Implications for early Himalayan orogeny and unroofing. Geological Society of America Bulletin, 113, 320-332.
Rahman, M.J.J., Suzuki, S., 2007. Geochemistry of sandstones from the Miocene Surma Group, Bengal Basin, Bangladesh: implications for Provenance, tectonic setting and weathering. Geochemical Journal, 41, 415–428.
Ranjan N., Banerjee D.M., 2009. Central Himalayan crystalline as the primary source for the sandstone-mudstone suites of the Siwalik Group: New geochemical evidence. Gondwana Research, 16, 687-696.
Roser, B.P., Korsch, R.J., 1988. Provenance signatures of sandstone–mudstone suites determined using discriminant function analysis of major-element data. Chemical Geology, 67, 119-139.
Sarwar, G., DeJong, K.A., 1979. Arcs, Oroclines, Syntaxes: the Curvatures of Mountain Belts in Pakistan. In: Farah, A., DeJong, K.A. (Eds.), Geodynamics of Pakistan. Geological Survey of Pakistan, Quetta, 341-349.
Suczek, C.A., Ingersoll, R.V., 1985. Petrology and provenance of Cenozoic sand from the Indus Cone and the Arabian Basin, DSDP Sites 221, 222, and 224. Journal of Sedimentary Petrology 55, 340-346.
Taylor, S.R., McLennan, S.M., 1985. The Continental Crust: its Composition and Evolution. Blackwell Scientific, Oxford.
Treloar, P.J., Izatt, C.N., 1993. Tectonics of the Himalayan collision between the Indian Plate and the Afghan block: a synthesis. In: Treloar, P.J., Searle, M.P. (Eds.),

Himalayan Tectonics. Geological Society of London, Special Publication 74, 69-87.

Van de Kamp, P.C., Leake, B.E., 1985. Petrography and geochemistry of feldspathic and mafic sediments of the northeastern Pacific margin. Transactions Royal Society of Edinburgh: Earth Science 76, 411-449.

Wronkiewicz, D.J., Condie, K.C., 1988. Geochemistry of Archean shales from the Witwatersrand Supergroup, South Africa: source-area weathering and provenance. Geochimica et Cosmochimica Acta, 51, 2401–2416.

Zuffa, G.G., 1980. Hybrid arenites: their composition and classification: Journal of Sedimentary Search, 50, 21-29.